Acta Pharmaceutica Sinica B 2022;12(2):735−746

Chinese Pharmaceutical Association
Institute of Materia Medica, Chinese Academy of Medical Sciences

Acta Pharmaceutica Sinica B

www.elsevier.com/locate/apsb
www.sciencedirect.com

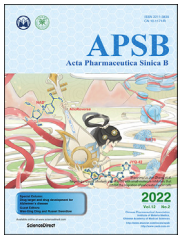

ORIGINAL ARTICLE

# The cell cycle inhibitor P21 promotes the development of pulmonary fibrosis by suppressing lung alveolar regeneration

**Xiaoxi Lv[a,*,†], Chang Liu[a,b,†], Shanshan Liu[a], Yunxuan Li[a], Wanyu Wang[a], Ke Li[c], Fang Hua[a], Bing Cui[a], Xiaowei Zhang[a], Jiaojiao Yu[a], Jinmei Yu[a], ZhuoWei Hu[a,*]**

[a]*Immunology and Cancer Pharmacology Group, State Key Laboratory of Bioactive Substance and Function of Natural Medicines, Institute of Materia Medica, Chinese Academy of Medical Sciences & Peking Union Medical College, Beijing 100050, China*
[b]*Drug Clinical Trial Institution, Children's Hospital, Capital Institute of Pediatrics, Beijing 100020, China*
[c]*Institute of Medicinal Biotechnology, Chinese Academy of Medical Sciences & Peking Union Medical College, Beijing 100050, China*

Received 21 April 2021; received in revised form 20 June 2021; accepted 9 July 2021

**KEY WORDS**

P21;
Cell senescence;
Alveolar epithelial type 2 cells;
Pulmonary fibrosis;
Alveolar regeneration;
Bleomycin;
Cell cycle arrest;
P300−$\beta$-catenin complex

**Abstract** The cell cycle inhibitor P21 has been implicated in cell senescence and plays an important role in the injury−repair process following lung injury. Pulmonary fibrosis (PF) is a fibrotic lung disorder characterized by cell senescence in lung alveolar epithelial cells. In this study, we report that P21 expression was increased in alveolar epithelial type 2 cells (AEC2s) in a time-dependent manner following multiple bleomycin-induced PF. Repeated injury of AEC2s resulted in telomere shortening and triggered P21-dependent cell senescence. AEC2s with elevated expression of P21 lost their self-renewal and differentiation abilities. In particular, elevated P21 not only induced cell cycle arrest in AEC2s but also bound to P300 and $\beta$-catenin and inhibited AEC2 differentiation by disturbing the P300−$\beta$-catenin interaction. Meanwhile, senescent AEC2s triggered myofibroblast activation by releasing profibrotic cytokines. Knockdown of *P21* restored AEC2-mediated lung alveolar regeneration in mice with chronic PF. The results of our study reveal a mechanism of P21-mediated lung regeneration failure during PF development, which suggests a potential strategy for the treatment of fibrotic lung diseases.

*Corresponding authors. Tel./fax: +86 10 83165034.
E-mail addresses: lvxiaoxi@imm.ac.cn (Xiaoxi Lv), huzhuowei@imm.ac.cn (ZhuoWei Hu).
[†]These authors made equal contributions to this work.
Peer review under responsibility of Chinese Pharmaceutical Association and Institute of Materia Medica, Chinese Academy of Medical Sciences.

https://doi.org/10.1016/j.apsb.2021.07.015

## 1. Introduction

Idiopathic pulmonary fibrosis (IPF) is a chronic, progressive respiratory disease primarily occurring in older adults, typically leading to death within 3−5 years[1,2]. Despite the multifactorial etiology of IPF, alveolar epithelial cell injury during the lung repair process plays prominent roles in the pathogenesis of this devastating disease. The sustained injury−repair process of the alveolar epithelium leads to myofibroblast activation. Abnormal remodeling of the lungs and architectural distortion cause gas exchange impairment and a progressive decline in lung function. At present, single intratracheal instillation of bleomycin (BLM)-induced mouse PF is the best characterized animal model[3]. The antitumor drug BLM exerts therapeutic efficacy by inducing DNA cleavage and reactive oxygen species (ROS) release with side effects of alveolar epithelium damage and PF development[4−6]. However, BLM-induced PF may exhibit different forms and severities depending on BLM stimulation times. Mice exposed to a single injection of BLM display acute inflammation and self-repair fibrotic lesions, whereas mice exposed to multiple BLM instillations show chronic inflammation and irreversible PF, which better mimic the pathological features observed in IPF patients[7]. Hence, understanding the cellular features of alveolar epithelial cells in distinct BLM models may provide a new perspective to clarify the pathogenesis and therapeutic options of IPF.

The lung is a complicated respiratory organ with a large and highly vascularized epithelial surface[8]. Alveoli are air-filled sacs lined by squamous alveolar epithelial type I cells (AEC1s) and cuboidal alveolar epithelial type II cells (AEC2s). As significant stem cells in alveoli, self-renewal and differentiation of AEC2s are closely associated with alveoli restoration. Regeneration of the alveolar epithelium plays a vital role in repairing gas-exchanging regions and the integrity of the alveolar structure, whereas impaired alveologenesis may cause severe lung function decline and final respiratory failure. When alveoli undergo sustained injury following various insults, AEC2s can proliferate or differentiate into AEC1s to restore impaired alveolar epithelium[9,10]. Multiple intratracheal administrations of BLM can repetitively damage the alveolar epithelium and may result in nonresolution PF due to the failure of lung regeneration[7].

Cellular senescence is a permanent state of cell cycle arrest and is correlated with age-associated diseases. Excessive accumulation of senescent cells in tissues can negatively modulate regenerative capacities and contribute to functional decline[11]. Pro-aging stressors, including telomere attrition, oxidative stress, DNA damage, and proteome instability, that induce cellular senescence are also implicated in IPF[12]. Damage accumulation in tissues enhances the activity of the cyclin-dependent kinase inhibitors $P16^{Ink4a}$ and/or $P53\text{-}P21^{Cip1/Waf1}$ to antagonize cyclin-dependent kinases and block the cell cycle[12,13]. P53 phosphorylated by kinases directly activates the expression of the target gene P21[14,15]. The upregulation of P21, which induces P53-dependent G1 phase arrest, is a critical marker of cellular senescence[16−19]. These key signaling elements of cellular senescence are also important in the maintenance of stem cell functions[20,21]. As one of the triggers of stem cell aging, cellular senescence affects the self-renewal and differentiation of stem cells[22], thus impeding the regenerative capacity of damaged tissues.

Repetitive lung injury is the premise of PF, and cellular senescence is critical for the pathogenesis of IPF. Fibroblasts and epithelial cells isolated from IPF patients express senescence-associated markers[12,23]. However, the correlation of lung injury and AEC2 senescence, as well as the regenerative capacities of AEC2s following lung injury, remain elusive. In this study, we investigated the capacity for alveolar regeneration by comparing the cell features of AEC2 senescence in single-dose BLM (sBLM) and multiple-dose BLM (mBLM) PF models. Our work reveals that P21-mediated AEC2 senescence impairs alveolar regeneration and interferes with the resolution of lung fibrosis in mBLM-induced PF mice.

## 2. Materials and methods

### 2.1. Antibodies

Commercially available antibodies were purchased from the following vendors. Anti-P21 (Santa Cruz Biotechnology, catalog sc-6246); biotin anti-CD45 (Biolegend, 103104); biotin anti-CD16/32 (Biolegend, 101303); biotin anti-CD31 (Biolegend, 102504); biotin anti-Ter119 (Biolegend, 116204); biotin anti-integrin $\beta$4 (Biolegend, 123603); anti-P300 (CST, 96377S); anti-$\beta$-catenin (CST, 9587S); anti-$\gamma$-H2AX (CST, 80312S); anti-pro-SPC (abcam, ab151332); anti-PDPN (abcam, ab236529); anti-HA (MBL, 561); anti-MYC (MBL, M047-3); anti-GFP (MBL, M048-3); streptavidin-PE (Biolegend, 405204); EpCAM-APC (Biolegend, 118214); donkey anti-mouse Alexa 488 (Life Technologies, A21206); donkey anti-rabbit Alexa 647 (Life Technologies, A31571); anti-HA (MBL, 561); anti-MYC (MBL, M047-3); anti-GFP (MBL, M048-3).

### 2.2. Pulmonary fibrosis models

To generate the mBLM PF model, mice were anesthetized by 400 mg/kg avertin intraperitoneally. BLM (Hanhui Pharmaceuticals Co., Ltd.) dissolved in 50 μL of LPS-free PBS (1 U/kg) was sprayed intratracheally every 14 days 6 times. Mice were sacrificed 21 and 45 days after the last BLM challenge. The sBLM model was generated by a single intratracheal instillation of BLM (3 U/kg). Mice were harvested on Day 21 and Day 45 after modeling. To overexpress *P21* in lung tissue, the mice were intratracheally instilled with lentivirus overexpressing *P21* ($1 \times 10^7$ TU/mouse). To knock down *P21* in the lung, the mice were intratracheally instilled with *P21*-shRNA lentivirus ($1 \times 10^7$ TU/mouse) 10 days after the first and last BLM challenges.

### 2.3. Lung function measurement

Mice were connected to a flexiVent pulmonary system (SCIREQ Inc., Montreal, Canada) under anesthesia. Mice were mechanically ventilated (tidal volume 10 mg/kg, positive end expiratory pressure (PEEP) 3 $cmH_2O$, ventilatory frequency 150 breaths/

min). Respiratory system compliance (Crs) was measured to evaluate lung function.

### 2.4. Isolation of AEC2s

Mice were anesthetized with 400 mg/kg avertin and dissected to expose the lungs and heart. Cardiac perfusion of the lungs was performed *via* the right ventricle. Then, dispase solution (Roche, catalog 4942078001) was infused followed by 1% low-melting agarose through tracheal cannulation. The lung was rinsed with sterile PBS and snipped into individual lobes. Lung lobes were digested for 45 min at room temperature (RT) on a rocker at 150 rpm (ZS-ARM, Huayuan Inc., Zhejiang, China). The lung parenchyma was gently teased to prepare a single cell suspension with the addition of 7 mL of complete DMEM as well as DNase I (Sigma−Aldrich, catalog D5025). The single cell prep was strained through 70 and 40 μm strainers. After lysis of red blood cells, the cell pellet was resuspended in complete DMEM containing DNase. Biotinylated antibodies, including anti-CD45, anti-CD16/32, anti-CD31, anti-Ter119 and anti-integrin $\beta$4, were added to the suspension, and the cells were incubated for 45 min on ice. After deletion of lineage-positive cells *via* magnetic separation, AEC2s were further enriched for streptavidin-PE-negative and EpCAM-APC-positive cells using fluorescence-activated cell sorting (BD FACS Aria III, San Jose, CA, USA).

### 2.5. AEC2s 3D culture

A total of 6000 treated AEC2s and 90,000 fibroblasts were suspended in complete medium and blended with Matrigel at a ratio of 1:1. The cocultured mixture was seeded into a Transwell chamber. The outer chamber was filled with 500 μL of complete medium, and the medium was changed every 2 days. Colonies formed by AEC2s were observed by microscope.

### 2.6. Coimmunoprecipitation and Western blotting

Cells were collected and centrifuged at 3000 rpm (Allegra$^{TM}$X-22R Centrifuge, Beckman Coulter Inc., USA) for 5 min. After lysis for 30 min on ice followed by high-speed centrifugation, 10% of lysate supernatant was set aside as input. The remaining supernatant was incubated with the indicated antibodies. The mixture was rotated during incubation overnight at 4 °C, and then protein A/G Plus-agarose beads (Santa Cruz) were added for another 2 h. After washing with PBS for 4 times, the immunocomplexes were boiled with SDS loading buffer for 10 min at 98 °C. Denatured lysates were subjected to SDS-polyacrylamide gel electrophoresis (SDS-PAGE) followed by immunoblotting analysis. Sample proteins were transferred onto PVDF membranes, blocked in 5% milk and incubated with primary antibodies as well as secondary antibodies. Proteins were visualized by an LAS4000 Image Station (General Electric Company Cleveland, OH, USA).

### 2.7. Histopathology and immunofluorescence staining

To examine lung histopathology, the left lobes of the lungs were perfused with 4% paraformaldehyde, embedded in paraffin and sectioned. The tissues were stained with Masson's trichrome. For immunofluorescence staining, frozen lung sections were fixed with 4% paraformaldehyde, permeabilized with 0.5% Triton X-100 at RT for 20 min, blocked (5% donkey serum or 3% BSA) at 37 °C for 1 h and incubated with the indicated primary antibodies overnight at 4 °C. After washing 3 times, the tissues were incubated with the corresponding secondary antibodies at RT, washed, and mounted using 4,6-diamidino-2-phenylindole (DAPI) for nuclear staining. Images were acquired on a confocal microscope (Leica Microsystems, TCS SP2, Heidelberg, GmbH).

### 2.8. Telomere Q-FISH assay

Paraffin-embedded tissue sections were used for the Q-FISH assay. After deparaffinization, tissues underwent antigen retrieval by immersion in 10 mmol/L sodium citrate buffer, pH 6.5, and heating in a microwave. Tissue samples were incubated in 0.01 mol/L HCl containing 1% pepsin (Thermo Fisher Scientific), washed and air-dried. Then, 10 mg/mL RNase solution (Shanghai Ze Ye Yu Biotech Co., Ltd.) was added, followed by wash and probe incubation. Tissues were treated with 0.3 μg/mL PNA FISH probe TelC-Cy3 (Panagene) suspended in buffer of 70% formamide, 30% water and 10 mmol/L Tris, pH 7.5, incubated at 78 °C for 10 min and then at RT overnight. Tissues were washed with formamide buffer and then PBS containing 0.1% Tween, followed by 3% BSA and 10% donkey serum treatment. Pro-SPC antibody was added for incubation at 4 °C overnight. Tissues were washed, incubated with secondary antibody, washed again and stained for nuclei using Prolong Gold Antifade Mounting Medium with DAPI (Invitrogen). Images were captured using a confocal microscope, and telomere signal intensity was quantified by ImageJ software.

### 2.9. RNA extraction and quantitative real time PCR (QPCR)

Total RNA was extracted from cell samples using an RNA extraction kit (Promega) according to the manufacturer's recommendations. cDNA templates were synthesized *via* reverse transcription reactions with a TransScript kit (TransGen). QPCR analyses were performed using SYBR® Green reagent (Kapa Biosystems) in triplicate on a LineGene 9620 apparatus (Bioer). All mRNA expression levels of the indicated genes were normalized against *Gapdh*.

### 2.10. Cell cycle analysis

To analyze the cell cycle, the cells were harvested and stained with Partec CyStain® DNA 1 step (Münster, Germany). The cells were later analyzed by flow cytometry (BD, San Jose, CA, USA).

### 2.11. Senescence-associated β-galactosidase staining

Cells were plated on glass coverslips and then detected with a senescence-associated $\beta$-galactosidase Staining Kit (BioVision Inc.) following the manufacturer's instructions.

### 2.12. SOD level detection

Cell lysates were added to 96-well plates, and the SOD level in cells was detected with a Superoxide Dismutase Activity Assay Kit (Abcam) following the manufacturer's instructions.

### 2.13. NADP/NADPH analysis

The NADP/NADPH ratio in cells was detected with an $NADP^+$/NADPH Assay Kit with WST-8 (Beyotime) following the manufacturer's instructions.

### 2.14. ROS detection

To detect ROS levels in cells, the cells were stained with DCFH-DA, and then ROS were detected with a fluorescence microscope (Olympus).

### 2.15. RNA sequencing and analysis

Total RNA from AEC2s of mice was obtained, and the RNA quantity and quality were measured using a NanoDrop ND-1000. Libraries were constructed according to standard Illumina protocols. The quality of the RNA and complementary DNA was monitored using an Agilent Bioanalyzer 2100, and sequencing was performed on an Illumina HiSeq 4000 by KangChen Biotech Company (Shanghai). The series numbers are GSE110479 and GSE16198 in this study.

### 2.16. Statistics

Data are expressed as the mean ± standard error of the mean (SEM). Comparisons between two groups were performed by unpaired two-tailed Student's *t*-test. One-way ANOVA with Bonferroni's multiple comparison test was used to analyze multiple groups with equal variances, and Kruskal-Wallis one-way ANOVA was used to analyze multiple groups with unequal variances. Generally, all assays were carried out with $n \geq 3$ biological replicates. $P < 0.05$ was considered statistically significant.

## 3. Results

### 3.1. mBLM lung injury induces P21-dependent senescence in AEC2s

By comparing the extent of PF in mice exposed to sBLM injury or mBLM injury, we found that although sBLM-treated mice showed significant fibrotic lesions on Day 21 postinjury, the injury sites disappeared on Day 45 after BLM instillation. However, in mBLM mice, PF lesions and collagen deposition existed continuously, and no improvement in architectural distortion was observed on Day 21 and Day 45 after the last BLM challenge (Fig. 1A and B and Supporting Information Fig. S1A−S1C). In comparison with mice treated with mPBS, the mRNA microarray analysis revealed enhanced expression of *Cdkn1a* (P21) but not *Cdkn2a* (P16) in AEC2s isolated from mBLM-challenged mice (Fig. 1C). To evaluate senescence of AEC2s *in vivo*, we isolated primary AEC2s from mBLM-challenged mice at different time points and stained them for senescence-associated $\beta$-galactosidase (SA $\beta$-gal). After sBLM injection, the number of AEC2s that stained positive for SA $\beta$-gal increased on Day 21 and showed an obvious decline on Day 45. However, in AEC2s from mBLM-treated mice, the incidence of cells positive for SA $\beta$-gal staining remained high even 45 days after instillation (Fig. 1D). The percentage of senescent AEC2s showed no significant differences on Day 21 and Day 45 in the mBLM group (Fig. 1D). P53−P21 pathway plays an important role in regulating cellular senescence. Combining the results of mRNA microarray analysis and the senescence state of AEC2s, we further detected the levels of p-P53 and P21 in AEC2s isolated from BLM-exposed mice. The p-P53 level was increased in AEC2s on Day 21 and Day 45 in the mBLM group, but only on Day 21 in the sBLM group (Fig. 1E). The mRNA levels of *P21* showed a declining trend after the initial ascent at various time points examined in the sBLM group. However, a continuous enhancement of *P21* levels was found as the number of mBLM administrations increased (Fig. 1F). The AEC2s from mBLM mice showed much higher expression of P21 protein than those from mPBS-treated mice, and there was a negative correlation between P21 expression and lung function in fibrotic mice (Fig. 1G). These data indicate that the induction of P21 and fibrotic lesions caused by sBLM are reversible, but repetitive stimulation of BLM can irreversibly induce P21-dependent cellular senescence of AEC2s.

### 3.2. mBLM exposure induces telomere shortening in AEC2s

To explore the upstream stressors of mBLM-induced AEC2 senescence, we performed RT-PCR to examine the telomere length of genomic DNA isolated from AEC2s. The telomere length of AEC2s derived from sBLM-exposed mice did not show a change compared with control mice, while telomeres were markedly shortened in AEC2s from mBLM-exposed mice (Fig. 2A). We also measured telomere length by quantitative fluorescence *in situ* hybridization (Q-FISH). Quantification analysis of Q-FISH showed similar telomere fluorescence intensity in pro-SPC$^+$ AEC2s in sBLM-treated mice compared with age-matched control mice. In contrast, the fluorescence was much less intense in pro-SPC$^+$ AEC2s in mBLM-treated mice (Fig. 2B). These findings indicate that telomere shortening is critical in the irreversible damage caused by repetitive stimulation of BLM. To further investigate the relationship of PF lesions and telomere length, mBLM lung sections containing healthy regions and adjacent fibrotic sites were analyzed (Fig. 2C). We found that the telomere fluorescence intensity was only decreased in AEC2s in fibrotic lesions of BLM-exposed mice (Fig. 2D). To examine the extent of DNA injury in AEC2s, we examined the level of phospho-H2AX ($\gamma$-H2AX), a marker of DNA damage[24], in lung sections from mice 45 days after mBLM or sBLM exposure. The lungs of mBLM-treated mice had elevated $\gamma$-H2AX foci in AEC2s. Quantitative analysis indicated that 40% of AEC2s were $\gamma$-H2AX-positive. In contrast, sBLM-challenged mice showed no increase in the percentage of $\gamma$-H2AX-positive AEC2s (Fig. 2E). These findings suggest that mBLM challenge induces telomere-mediated senescence in AEC2s through DNA damage.

### 3.3. mBLM induces ROS generation in fibrotic AEC2s

Previous works have shown that the ROS−P53−P21 signaling pathway plays a significant role in cellular senescence. We speculated whether ROS content in AEC2s differs in sBLM and mBLM models. In AEC2s from sBLM mice, the ratio of oxidized coenzyme II (NADP)/reduced NADP$^+$ (NADPH) was elevated on Day 21 and returned to baseline levels on Day 45 post injury. Consistent with other biomarkers of senescence, a high NADP/NADPH ratio was sustained at different time points in the mBLM model (Fig. 3A). The level of superoxide dismutase (SOD) declined in fibrotic AEC2s on Day 21 post sBLM exposure, but the SOD level rebounded on Day 45. However, the continuously low level of SOD in mBLM-treated mice supported sustained ROS accumulation in fibrotic AEC2s (Fig. 3B). In addition, we measured the level of ROS by flow cytometry analysis and fluorescence (Fig. 3C and D). The rebound trend of ROS in AEC2s from sBLM mice and continuous accumulation of ROS in fibrotic AEC2s from mBLM mice were consistent with the corresponding ratio of NADP/NADPH as well as SOD activity. These data

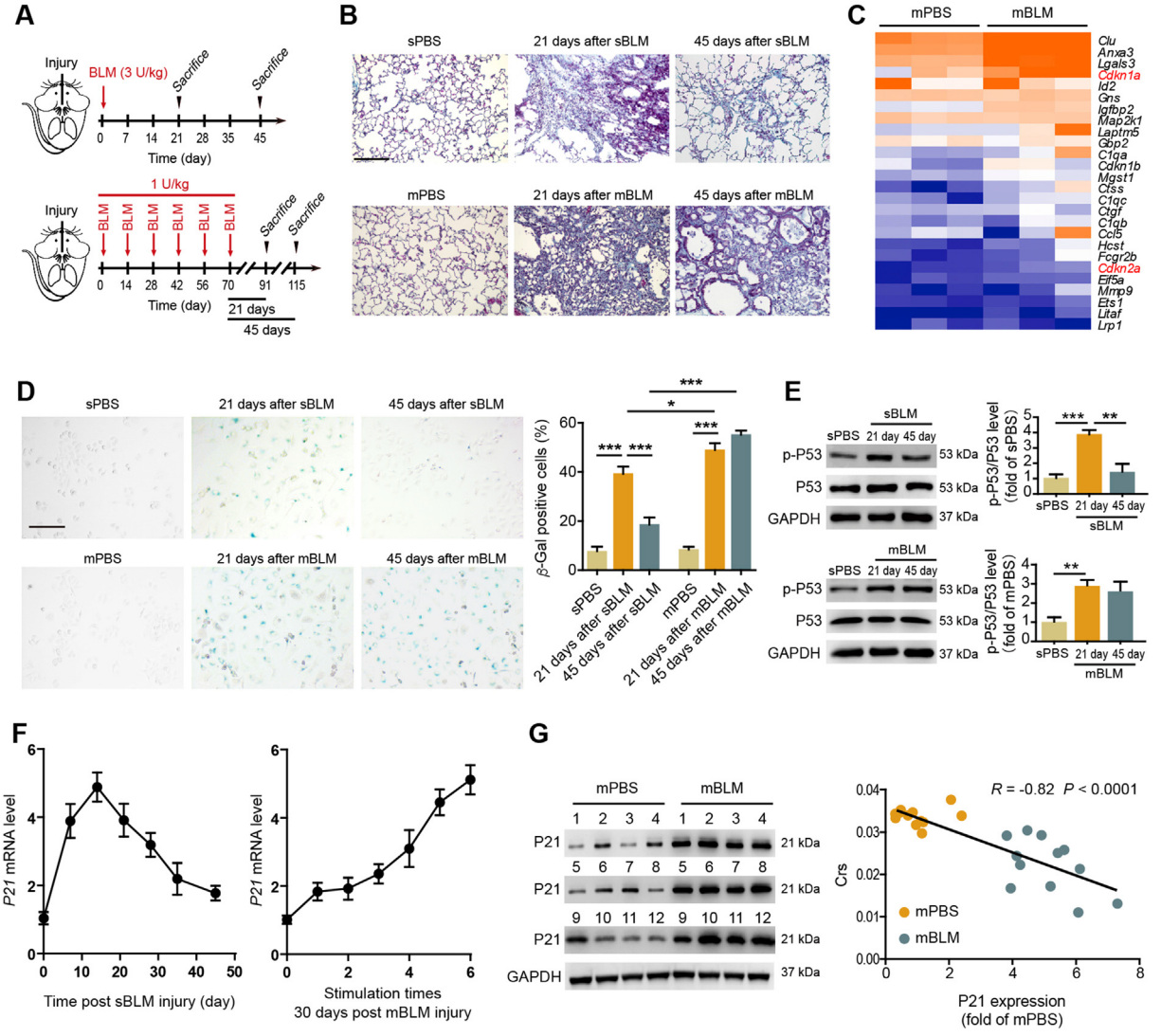


**Figure 1** mBLM injury induces P21 dependent senescence in AEC2s. (A) The schematic diagram for evaluating the fibrotic change in sBLM and mBLM models. The mice were sacrificed by excessive anesthesia on Day 21 or Day 45 after the last BLM challenge. (B) Masson staining was performed to evaluate fibrotic changes in lungs from sBLM or mBLM-exposed mice ($n = 6$). Scale bars, 200 μm. (C) Gene expression profiles by RNA-seq show that senescence-related genes were up regulated in AEC2s isolated form mBLM group ($n = 3$). The color scale indicates the log2 ratio of the normalized RNA-seq value intensities. (D) β-Gal staining was performed to evaluate the senescence in AEC2s isolated from indicated mice. Scale bars, 200 μm ($n = 6$). (E) Sample immunoblots of the expression of p-P53 and P53 in AEC2s isolated from different mice ($n = 3$). (F) RNA levels of *P21* in AEC2s from mice at the indicated days post sBLM or mBLM challenges ($n = 3$). (G) Correlation between P21 expressions and lung functions after mBLM challenge. The *Y*-axis denotes the lung function, and the *X*-axis denotes the relative P21 expression. Each point represents the value from one mouse. The *P* value was calculated with Spearman's rank correlation test in the mBLM group ($n = 12$). Data are represented as mean ± SEM. Statistical significance among groups was determined by one-way ANOVA. $^{*}P < 0.05$, $^{**}P < 0.01$, $^{***}P < 0.001$.

indicate that mBLM exposure induces sustained ROS elevation along with P53-dependent P21 enhancement in fibrotic AEC2s.

### 3.4. *P21 inhibits self-renewal and differentiation of AEC2s*

To explore the regenerative capacity of senescent AEC2s, we measured the mRNA levels of *Sftpa*, *Sftpb*, *Sftpc* and *Sftpd* in AEC2s from the indicated mice to evaluate surfactant production. Relevant mRNA levels of these genes in sBLM mice were reduced on Day 21 and recovered slightly on Day 45 after BLM instillation (Fig. 4A). In contrast, these surfactant-related genes were decreased in AEC2s from mBLM mice at both time points, which demonstrated that irreversible damage caused dysregulation of surfactant production (Fig. 4A). Because P21 was found to accumulate persistently in fibrotic AEC2s, we speculated whether the elevation of P21 causes stemness dysfunction of AEC2s. To evaluate the stemness of AEC2s, AEC2s from mice instilled with P21-overexpressing adenovirus (*P21*-Ad) were cocultured with fibroblasts in a 3D coculture system. The number and size of colonies formed by *P21*-Ad-treated AEC2s were significantly lower than those formed by *Con*-Ad-treated cells (Fig. 4B–D), suggesting that overexpression of *P21* inhibits the self-renewal capacity of AEC2s. Furthermore, the morphological changes of the *P21*-overexpressing AEC2s in 2D culture conditions and the

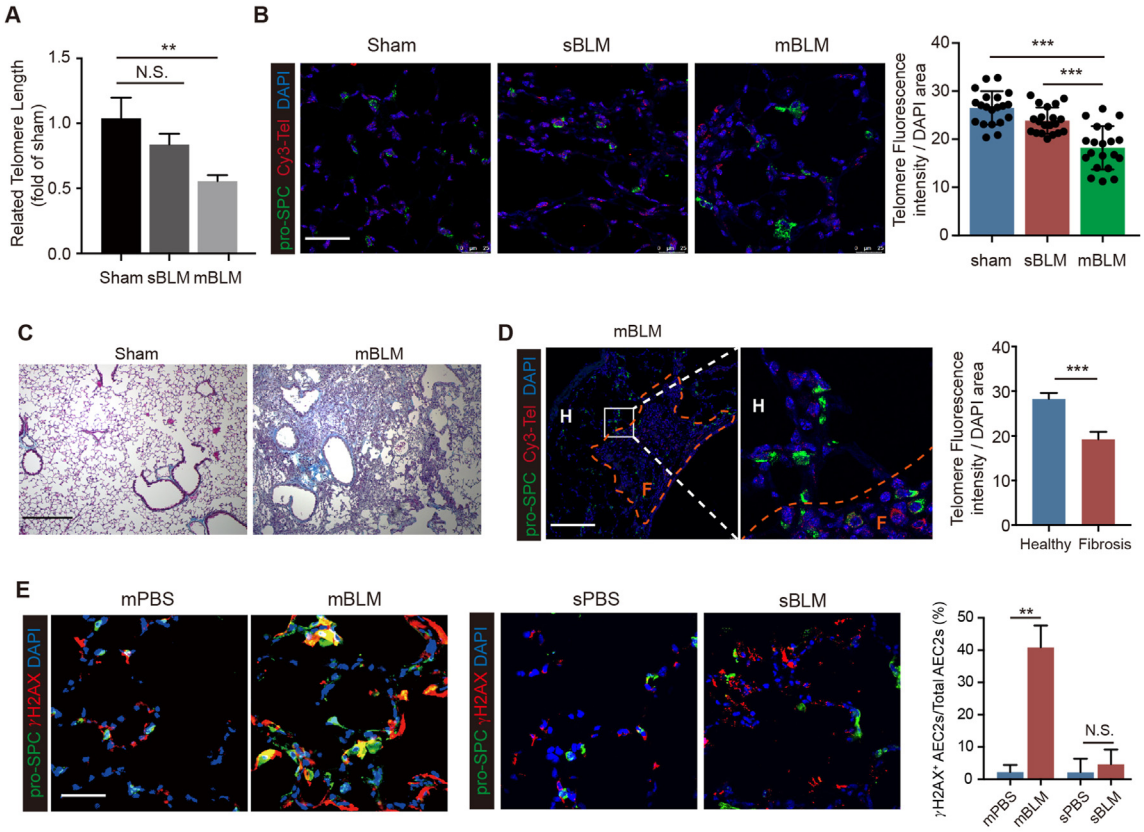


**Figure 2** mBLM exposure induces telomere shortening in AEC2s. (A) QPCR analyses were performed to evaluate the telomere length in AEC2s isolate form indicated mice ($n = 5$). (B) Q-FISH assay were performed to evaluate the telomere length in AEC2s in different mice lung tissue. Scale bars, 50 μm ($n = 20$). Masson staining (C) and Q-FISH assay (D) were performed to evaluate the telomere length in AEC2s in fibrotic lung tissue sand healthy lung tissues. Scale bars, 200 μm in (C) and 50 μm in (D) ($n = 5$). (E) Confocal images showing the pro-SPC and γH2AX expression in lung tissues from mice 45 days post mBLM or sBLM challenging. Scale bars, 50 μm ($n = 5$). Data are represented as mean ± SEM. Statistical significance between the two groups was determined by unpaired two-tailed Student's *t*-test; Statistical significance among groups was determined by one-way ANOVA. $^{**}P < 0.01$, $^{***}P < 0.001$; N.S., non-significance.

decreasing level of AQP5 in *P21*-overexpressing AEC2s showed a significantly decreased differentiation capacity relative to squamous AEC1s (Fig. 4E and F). To further confirm the inhibitory effects of P21 on AEC2 stemness, we performed RT-PCR analyses to measure the RNA levels of stemness marker genes related to AEC1s and AEC2s. We found that these marker genes were all evidently decreased in *P21*-overexpressing AEC2s (Fig. 4G). WNT signaling is critical for lung development, homeostasis and lung alveolar regeneration post injury[25]. The RNA-seq results indicated that the cell senescence pathway was activated and that the WNT signaling pathway was suppressed in *P21*-overexpressing AEC2s (Fig. 4H). These data indicate that elevation of P21 expression suppresses the capacity for self-renewal and differentiation in AEC2s.

To evaluate whether P21 expression is relevant to profibrotic cytokine secretion in AEC2s, bronchoalveolar lavage fluid in the lungs was harvested on Day 45 after sBLM or mBLM injury. Compared with AEC2s from sBLM mice, pro-fibrotic cytokines, including IL-1$\beta$ and TGF-$\beta$1, were found to be increased in the mBLM group (Fig. 4I). To examine whether AEC2s exert a profibrotic impact on fibroblasts, we cocultured AEC2s isolated from the indicated mice with primary lung fibroblasts in a Transwell system. Crystal violet staining and corresponding quantification revealed much greater migration of fibroblasts when these cells were cocultured with fibrotic AEC2s (Fig. 4J), which suggests that *P21*-overexpressing AEC2s secrete profibrotic cytokines into the supernatant to promote the migration of fibroblasts.

### 3.5. *P21 suppresses self-renewal of AEC2s by inducing cell cycle arrest*

As a key signaling component of the senescence machinery, P21 can arrest cell cycle progression. Thus, we sought to determine whether overexpression of *P21* induces cell cycle arrest in AEC2s. We analyzed different phases of the cell cycle in *P21*-Ad-treated AEC2s and *Con*-Ad-treated AEC2s by flow cytometry. Compared with cells in the control group, *P21*-overexpressing AEC2s exhibited cell cycle arrest in the G0/G1 phase. Quantification revealed that the percentage of AEC2s in the population significantly increased in G0/G1 phase after *P21*-Ad treatment (Fig. 5A). Then, similar arrest at G0/G1 of the cell cycle was identified in AEC2s from mBLM-exposed mice but not in age-matched sham mice, confirming that a high level of P21 is closely related to self-renewal failure in fibrotic AEC2s (Fig. 5B). These findings indicate that elevated P21 caused by mBLM exposure induces cycle arrest of stress-responsive AEC2s in the G0/G1 phase and regenerative dysfunction.

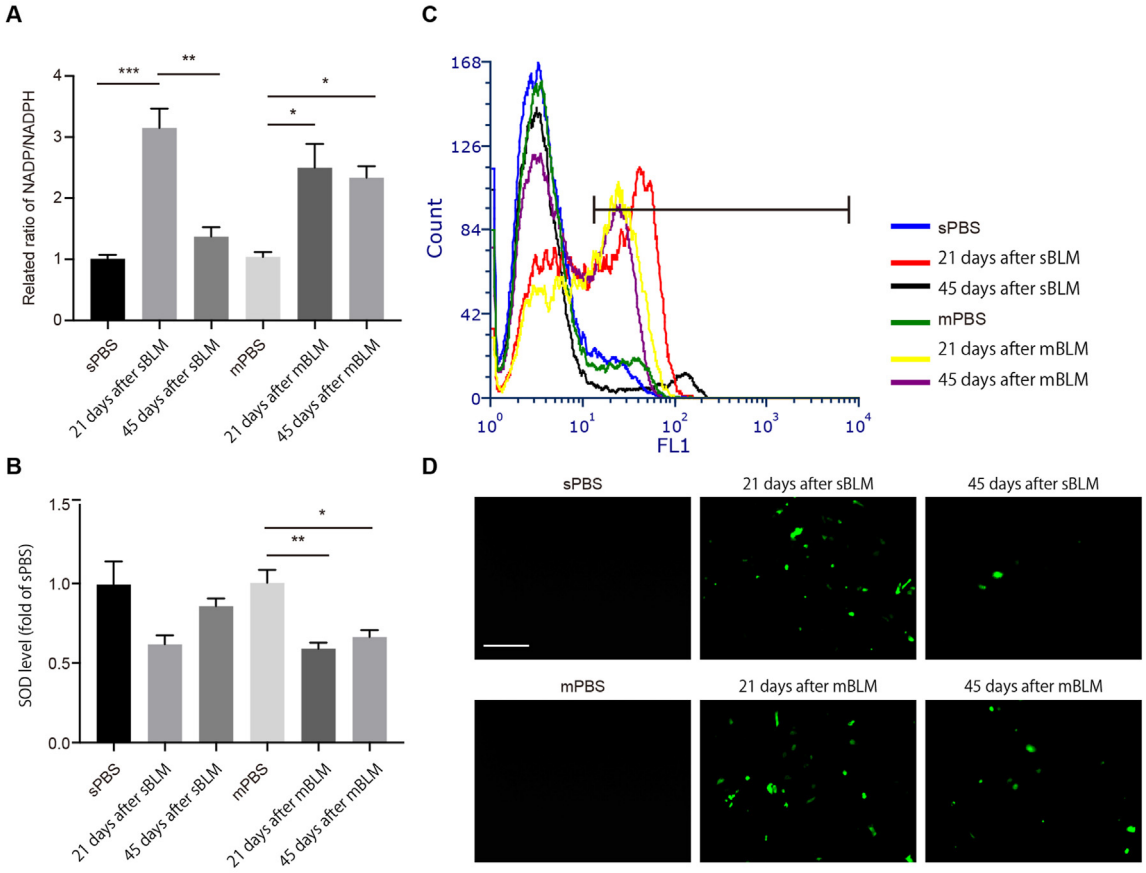


**Figure 3** Sustained ROS induces P53-dependent P21 expression in AEC2s. (A) The level of NADP/NADPH was measured in AEC2s isolated from indicated mice ($n = 3$). (B) The SOD level was measured in AEC2s isolated from indicated mice ($n = 3$). (C) Flow cytometry analysis was performed to evaluate ROS level in AEC2s isolated from indicated mice after incubation with DCFH-DA probe ($n = 3$). (D) Confocal analysis was performed to evaluate ROS level in AEC2s isolated from indicated mice after incubation with DCFH-DA probe. Scale bars, 50 μm ($n = 4$). Data are represented as mean ± SEM. Statistical significance among groups was determined by one-way ANOVA. $^{*}P < 0.05$, $^{**}P < 0.01$, $^{***}P < 0.001$.

### *3.6. P21 inhibits AEC2 differentiation by disturbing the P300−β-catenin interaction*

To explore the mechanisms involved in P21-mediated AEC2 differentiation failure, we examined the expression of the AEC1 marker PDPN and the AEC2 markers pro-SPC and P21 in AEC2s from mBLM mice. The level of PDPN was increased and pro-SPC was decreased in AEC2s isolated from mPBS mice in the 2D culture system. However, high levels of P21 and unchanged levels of PDPN and pro-SPC were found in AEC2s isolated from mBLM mice after 4 days of culture (Fig. 5C). The different trends of P21 and the two marker genes support the previous notion that P21 suppresses the self-renewal and differentiation of AEC2s. Given that the P300−β-catenin interaction was reported to demonstrate a close relationship with AEC2 differentiation[25], we immunoprecipitated the β-catenin protein to examine the endogenous P300−β-catenin interaction in AEC2s of mBLM mice. Elevated expression of P21 and a reduced P300−β-catenin interaction were observed in AEC2s from mBLM mice, suggesting that mBLM-induced P21 enhancement breaks the P300−β-catenin interaction during progression of PF (Fig. 5D). Overexpression of *P300*, β-catenin and *P21* constructs in HEK293T cells also decreased the P300−β-catenin interaction, supporting a critical role for P21 as an inhibitor of the P300−β-catenin interaction in the context of AEC2 differentiation (Fig. 5E). To further determine the interaction domain of P21 and the P300−β-catenin complex, we constructed truncation mutants of the N-terminal domain (ΔC, aa1−aa100) and the C-terminal domain (ΔN, aa100−aa159) of P21 protein in an HA-tagged expression vector. Two truncation mutants were cotransfected with β-catenin or P300. Co-IP analyses showed that β-catenin interacted with the N-terminal domain of P21 and that P300 bound to the C-terminal domain, indicating that P21 and the P300−β-catenin complex form a heterogeneous trimer (Fig. 5F and G). Additionally, the expression of AXIN 2, a classical target gene of β-catenin, was reduced in *P21*-overexpressing AEC2s (Fig. 5H and I). These data suggest that P21 inhibits AEC2 differentiation by breaking the P300−β-catenin interaction.

### *3.7. Knockdown of P21 attenuates mBLM-induced pulmonary fibrosis*

To further verify the role of P21 in lung alveolar regeneration and PF, we knockdown *P21* in AEC2s isolated from the mBLM mice. The self-renewal (Supporting Information Fig. S2A and S2B) and the differentiation (Fig. S2C and S2D) ability of AEC2s were increased after knockdown *P21* in fibrotic AEC2s. In addition, *P21* was silenced in lung tissues by instillation of *P21*-shRNA lentivirus. We found that knockdown of P21 expression in lung tissue reduced fibrotic changes, as indicated by relieved septal

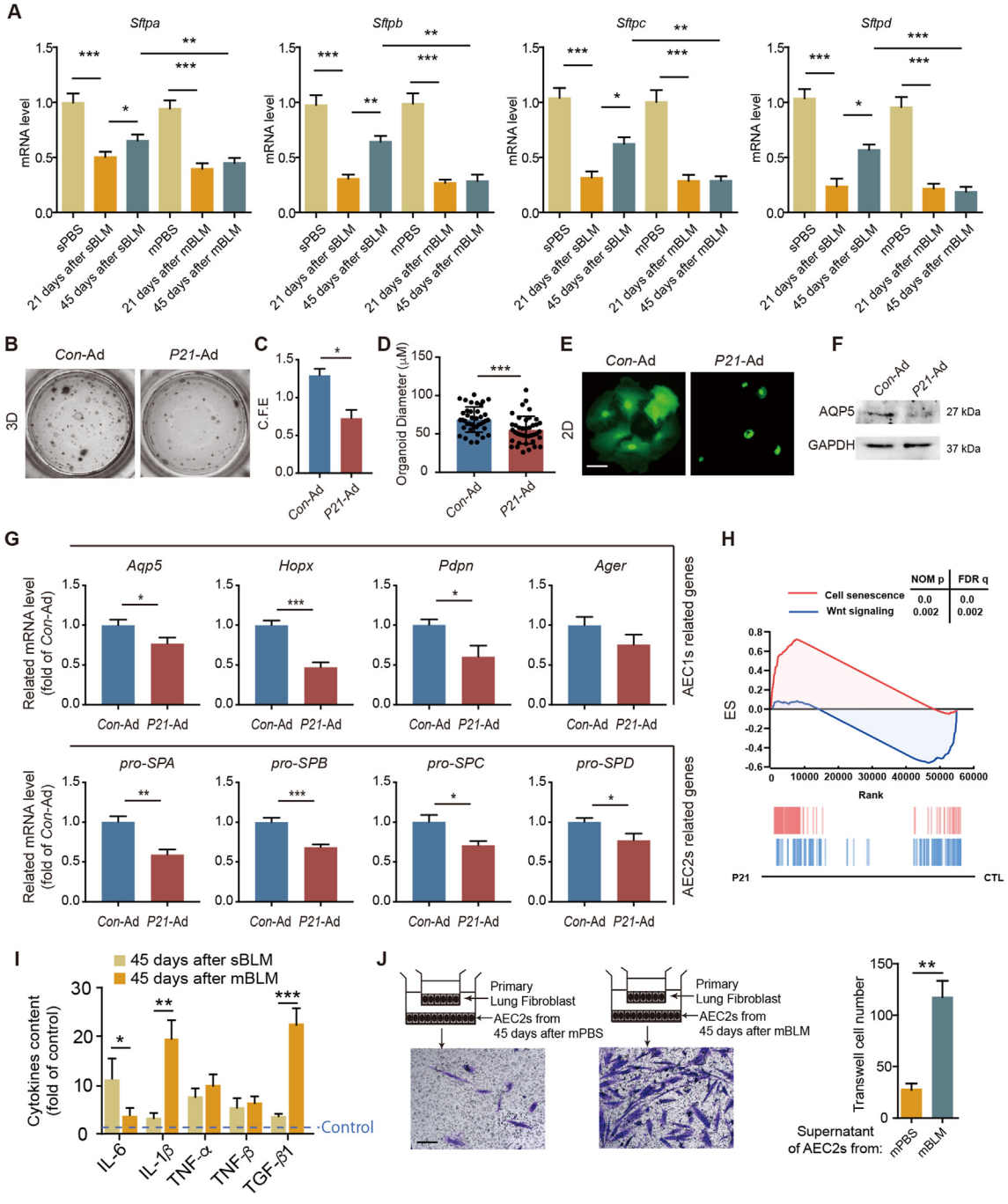


**Figure 4** P21 inhibits self-renewal and differentiation of AEC2s. (A) The mRNA expressions of surfactants in AEC2s isolated from indicated mice ($n = 3$). (B) Images of the indicated AEC2 colonies growing in the 3D co-culture system ($n = 3$). (C) The colony-forming efficiency of AEC2s sorted from *Con*-Ad- or *P21*-Ad-infected mice ($n = 5$). (D) Colony sizes of AEC2s from *Con*-Ad- or *P21*-Ad-infected mice ($n = 40$). (E) Images of the indicated AEC2 colonies growing in the 2D co-culture system. Scale bars, 40 μm ($n = 3$). (F) Sample immunoblots of the expression of AQP5 in *Con*-Ad- or *P21*-Ad-infected AEC2s ($n = 3$). (G) The mRNA expressions of the AEC1- or AEC2- related genes in *P21* overexpressed AEC2s ($n = 3$). (H) Gene set enrichment analysis (GSEA) identifies P21-regulated gene networks associated with senescence and WNT signaling pathway ($n = 3$). (I) Analyses of the pro-fibrotic cytokines released from AEC2s isolated from indicated mice in the culture supernatants ($n = 3$). (J) Quantitative analyses of Transwell assays show that the supernatants from indicated AEC2s enhanced the migration of lung fibroblasts. Scale bars, 400 μm ($n = 5$). Data are represented as mean ± SEM. Statistical significance between the two groups was determined by unpaired two-tailed Student's *t*-test; Statistical significance among groups was determined by one-way ANOVA. $^{*}P < 0.05$, $^{**}P < 0.01$, $^{***}P < 0.001$.

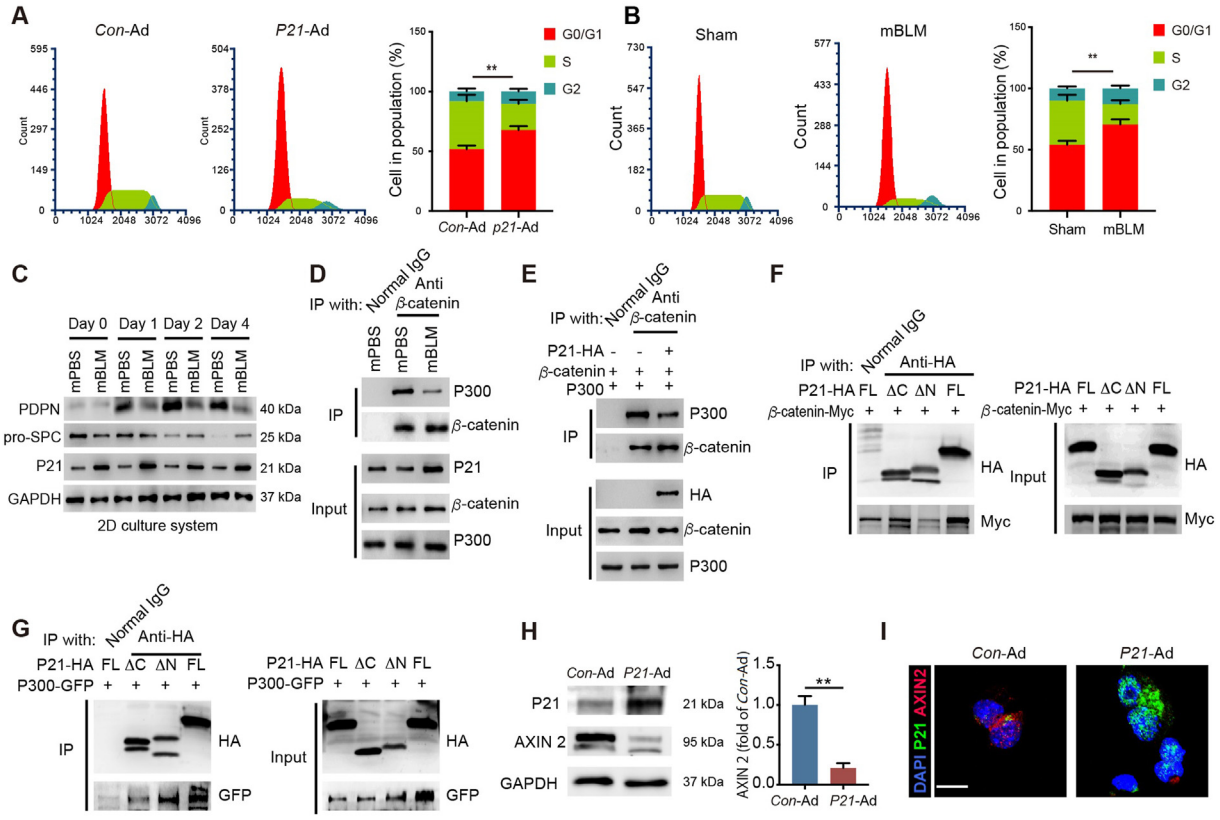


**Figure 5** P21 inhibits self-renewal and differentiation of AEC2. (A) The DNA profile of the *Con*-Ad or *P*21-Ad treated AEC2s were examined by flow cytometry ($n = 3$). (B) The DNA profile of the AEC2s isolated from indicated mice were examined by flow cytometry ($n = 3$). (C) Sample immunoblots of the expression of the indicated proteins in AEC2s isolated from different mice ($n = 3$). (D) IP assay analyses of the P300−β-catenin interaction in AEC2s. Cells extracts were IP with normal IgG or anti-β-catenin antibody (Ab) and blotted with anti-P300 Ab ($n = 3$). (E) IP assay analyses of the P300−β-catenin interaction in HEK293T cells after indicated treatment. Cells extracts were IP with normal IgG or anti-β-catenin Ab and blotted with anti-P300 Ab ($n = 3$). (F) Mapping of P21 regions involved in β-catenin binding. HEK 293T cells were co-transfected with indicated constructs of *P21* and β-catenin−*Myc*. Cell extracts were IP with anti-HA Ab and blotted with MYC Ab ($n = 3$). (G) Mapping of P21 regions involved in P300 binding. HEK293T cells were co-transfected with indicated constructs of *P21* and *P300-GFP*. Cell extracts were IP with anti-HA Ab and blotted with GFP Ab ($n = 3$). (H) The expression of P21 and AXIN 2 in AEC2s after indicated treatment ($n = 3$). (I) the level of P21 and AXIN 2 in AEC2s were observed with confocal assay. Scale bars, 10 μm ($n = 5$). Data are represented as mean ± SEM. Statistical significance between the two groups was determined by unpaired two-tailed Student's *t*-test. $^{**}P < 0.01$.

thickening and alveolarization (Fig. 6A). The fibrotic score was lower in the *P21* knockdown group than in the *Con* virus group after mBLM injury (Fig. 6B). Additionally, lung function was improved after silencing *P21* expression in fibrotic lung tissue (Fig. 6C). Moreover, silencing *P21* expression not only decreased the hydroxyproline content in lung tissue (Fig. 6D) but also enhanced the colony-forming efficiency of AEC2s isolated from fibrotic mice (Fig. 6E). In summary, telomere shortening, DNA damage and ROS accumulation caused by mBLM exposure activate the P53−P21 signaling pathway. Elevated P21 expression induces G0/G1 growth arrest and inhibits self-renewal of AEC2s. Meanwhile, the functional interaction between P300 and β-catenin is blocked by enhanced P21. As a result, the accumulated P21 mediates dysfunction of AEC2s and leads to lung regeneration failure in the progression of PF (Fig. 6F).

## 4. Discussion

Although sBLM intratracheal administration-induced mouse PF is the classic animal model for studying IPF, this model only causes acute inflammation and reversible fibrotic changes following BLM-induced acute lung injury. In contrast, the mBLM mouse model exhibits better mimesis of clinical IPF patients with the features of sustained inflammation and irreversible PF changes. In this study, we emphatically analyzed the functional variations of AEC2s after acute and chronic lung injury in these two PF models. We found that the expression of P21, a prominent protein that modulates cell cycle progression and DNA-damage response (DDR)[26], and the activity of senescence-associated signaling were enhanced in AEC2s from mBLM mice but not in AEC2s from sBLM mice, which is consistent with *in vitro* observations reported previously[27]. Moreover, repeated injury of AEC2s resulted in telomere shortening and triggered P21-dependent cell senescence. AEC2s with high P21 expression lost the ability to undergo self-renewal and differentiation, which resulted in the non-resolution of chronic inflammation and PF (Fig. 6F). Our study thus reveals a mechanism of P21-mediated lung regeneration failure during PF development, which may offer a potential strategy for the treatment of fibrotic lung diseases.

Repetitive injection of BLM can induce cellular senescence of AEC2s, and one significant inducer of senescence is telomere dysfunction. Clinical IPF patients exhibit telomere shortening in

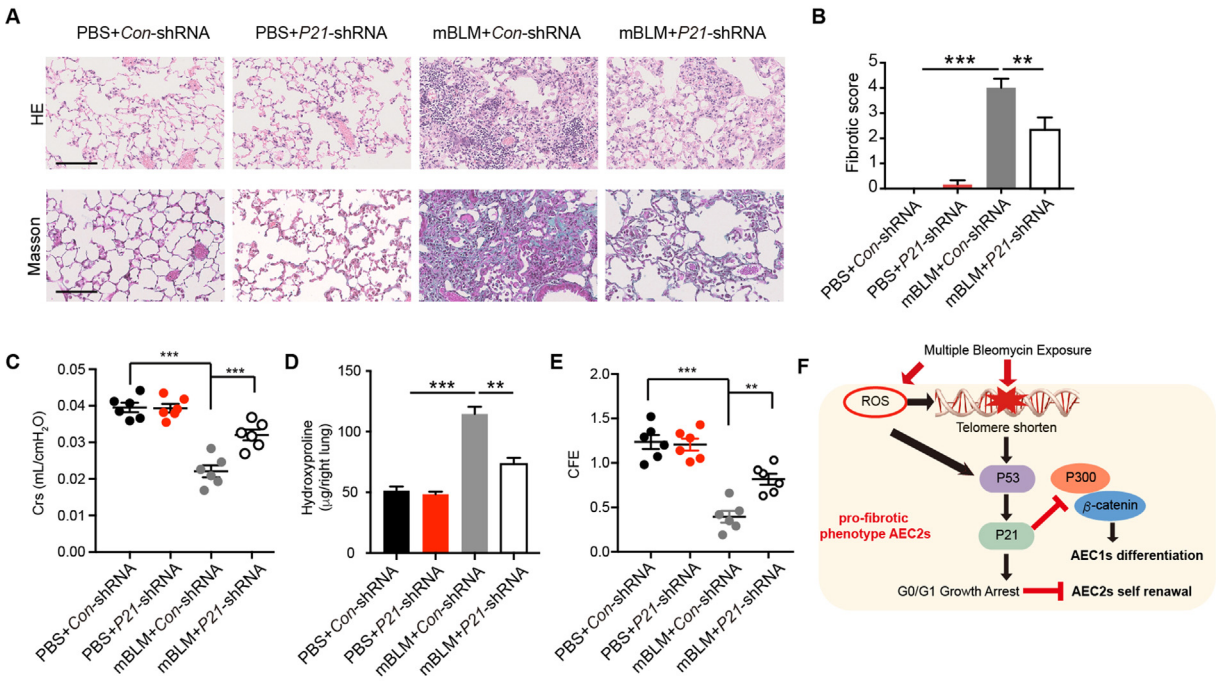


**Figure 6** Knockdown P21 attenuates mBLM induced pulmonary fibrosis. (A) HE (up) and Masson staining (down) were assessed to evaluate fibrotic change in indicated mice. Scale bars, 200 μm ($n = 6$). (B) Fibrotic score of mice after indicated treatment ($n = 6$). Crs (C) and hydroxyproline content in the right lung (D) were assessed to evaluate lung function and pulmonary fibrosis ($n = 6$). (E) The colony-forming efficiency of AEC2s from indicated mice ($n = 6$). (F) Schematic diagram illustrates that mBLM induced ROS and telomere shorten trigger P21 mediated senescence and promote the development of pulmonary fibrosis by inhibiting lung regeneration. Data are represented as mean ± SEM. Statistical significance among groups was determined by one-way ANOVA. $^{**}P < 0.01$, $^{***}P < 0.001$.

AEC2s[28]. Moreover, conditional deletion of telomere repeat binding factor in AEC2s was found to induce pulmonary fibrosis in mice directly[29]. Telomere dysfunction can trigger the typical DDR, which enables cells to sense damaged DNA, such as double-strand breaks, arrest cell cycle progression and repair damage, and this process is usually accompanied by P21 deposition[15]. BLM acts by embedding in DNA to induce DNA strand cleavage and subsequent DDR, and telomere shortening is similar to double-strand breaks. Our results reveal elevated staining for γ-H2AX and telomere shortening in AEC2s isolated from mBLM-treated mice. We propose that repetitive stimulation of BLM triggers DDR by cutting telomeres of AEC2s and that subsequent activation of the P53−P21 signaling pathway results in P21 deposition in senescent AEC2s. Telomeres are tandem DNA repeats of TTAGGG structures at the end of chromosomes, and this sequence is very sensitive to various damage. Shortened telomeres can activate P21 through P53 dependent pathway[30]. In contrast to sBLM stimulation, repetitive DNA damage alone can induce telomere dysfunction in mice, mainly because the telomere length of mice is much longer than that of humans. Meanwhile, this suggests that repetitive damage caused by BLM more closely resembles the practical situation in clinical cases. Oxidative stress was reported to be closely associated with DDR and cellular senescence, and there is evidence showing the involvement of ROS accumulation in pulmonary fibrosis pathogenesis[31,32]. Our results reveal that AEC2s from mBLM-treated mice maintained high levels of ROS, but sBLM injection-induced enhancement of ROS in AEC2s showed regression on Day 45 after administration. Our findings suggest the simultaneous induction of ROS increases during the process of telomere dissection by BLM treatment to activate P53−P21 signaling.

PF is the pathological structure of incurable fibroproliferative lung diseases that are attributed to the repeated lung injury-caused failure of lung alveolar regeneration. The repeated injury to the lung causes chronic inflammation and irreversible fibrotic change, suggesting that failure of lung alveolar regeneration is an important mechanism in progressive PF. Several types of cells are involved in lung regeneration, such as $P63^{+}KRT5^{+}$ distal airway stem cells[33]. However, AEC2s, which have secretory, host defense, self-renewal and differentiation ability, are primary alveolar stem cells maintaining lung homeostasis[34]. When alveoli undergo sustained damage, AEC2s can differentiate into AEC1s under the impact of the alveolar microenvironment to restore the integrity of the alveolar epithelium. Hence, further investigation of cellular phenotypes and changes in signaling pathways in fibrotic AEC2s offers a better understanding of IPF pathogenesis. Cellular senescence is a stress-responsive procedure of cell cycle arrest, and senescence of stem cells is closely correlated with tissue regeneration failure. In this study, we found that overexpression of P21 impairs the stemness of AEC2s. The stem cells showed decreased capacities for self-renewal and differentiation after P21 overexpression *in vitro*, which is consistent with the cellular behavior of P21-elevated AEC2s isolated from mBLM-exposed mice. Indeed, recent studies indicate that P21 can arrest the transition of G1−S phase in the cell cycle by inhibiting cyclin-dependent kinase following DNA damage[16]. We found that overexpression of P21 impeded the self-renewal of AEC2s *via* G1 phase arrest in the cell cycle. The WNT signaling pathway is involved in the development of many organs and contributes to homeostasis maintenance and injury repair[35]. The activation of the classical WNT/β-catenin pathway will induce β-catenin enters into nucleus and promotes the translation of epithelial−mesenchymal transition (EMT) related genes, thus

accelerating EMT process[36]. Although, recent study identified that EMT cell is not the main source of myofibroblast in PF[37], dysregulated WNT/$\beta$-catenin pathway induces dysfunction of AEC2s. In particular, the WNT signaling-associated modulation of target gene transcription in various stem cells plays a critical role in regulating cellular behavior. After WNT signaling pathway activation, P300−$\beta$-catenin but not CBP−$\beta$-catenin interplay promotes AEC2-to-AEC1 differentiation[25]. Moreover, we found that the N-terminal domain and the C-terminal domain of P21 bind to $\beta$-catenin and P300, respectively, to disrupt the P300−$\beta$-catenin interaction and repress AEC2-to-AEC1 differentiation. Our work thus shows that the WNT signaling pathway mediates P21 elevation, impeding the self-renewal and differentiation of AEC2s into AEC1s.

## 5. Conclusions

The current study provides insight into the pathogenesis and potential therapeutic strategy of IPF. Indeed, excessive accumulation of P21 in alveolar stem cell AEC2s impedes self-renewal of AEC2s by inducing G1 phase arrest in the cell cycle and inhibits AEC2-to-AEC1 differentiation. This study may help us to modulate the regenerative capacities of AEC2s by reducing cellular P21 levels for better therapeutics in IPF patients.

## Acknowledgments

This work was supported by grants from National Key R&D Program of China (2017YFA0205400), National Natural Science Foundation of China (81773781 to Zhuowei Hu; 81503128 to Xiaoxi Lv), and from CAMS Innovation Found for Medical Sciences (2016-I2M-1-007 to Zhuowei Hu, Fang Hua; 2016-I2M-1-008 to Xiaoxi Lv; 2016-I2M-1-011 to Ke Li; 2016-I2M-3-008 to Bing Cui, Shanshan Liu, Jiaojiao Yu, and Jinmei Yu, China).

## Author contributions

Zhuowei Hu and Xiaoxi Lv raised conceptions and participated in the overall design, supervision and coordination of the study. Xiaoxi Lv and Chang Liu designed and performed most of experiments. Shanshan Liu, Yunxuan Li, Wanyu Wang, Ke Li, Fang Hua, Jiaojiao Yu, and Jinmei Yu. participated in molecular and cellular biological experiments. Bing Cui., and Xiaowei Zhang performed animal studies. Zhuowei Hu, Xiaoxi Lv and Chang Liu wrote the manuscript. All authors read and approved the manuscript.

## Conflicts of interest

The authors have no conflicts of interest to declare.

## Appendix A. Supporting information

Supporting data to this article can be found online at https://doi.org/10.1016/j.apsb.2021.07.015.

## References

1. American Thoracic Society. Idiopathic pulmonary fibrosis: diagnosis and treatment. International consensus statement. American Thoracic Society (ATS), and the European Respiratory Society (ERS). *Am J Respir Crit Care Med* 2000;**161**:646−64.
2. Raghu G, Remy-Jardin M, Myers JL, Richeldi L, Ryerson CJ, Lederer DJ, et al. Diagnosis of idiopathic pulmonary fibrosis. An official ATS/ERS/JRS/ALAT clinical practice guideline. *Am J Respir Crit Care Med* 2018;**198**:e44−68.
3. Moore BB, Hogaboam CM. Murine models of pulmonary fibrosis. *Am J Physiol Lung Cell Mol Physiol* 2008;**294**:152−60.
4. Walters DM, Kleeberger SR. Mouse models of bleomycin-induced pulmonary fibrosis. *Curr Protoc Pharmacol* 2008;**40**. 5.46.1-17.
5. Muggia FM, Louie AC, Sikic BI. Pulmonary toxicity of antitumor agents. *Cancer Treat Rev* 1983;**10**:221−43.
6. Chen J, Stubbe J. Bleomycins: towards better therapeutics. *Nat Rev Cancer* 2005;**5**:102−12.
7. Liu SS, Lv XX, Liu C, Qi J, Li YX, Wei XP, et al. Targeting degradation of the transcription factor C/EBP$\beta$ reduces lung fibrosis by restoring activity of the ubiquitin-editing enzyme A20 in macrophages. *Immunity* 2019;**51**:522−34.
8. Barkauskas CE, Cronce MJ, Rackley CR, Bowie EJ, Keene DR, Stripp BR, et al. Type 2 alveolar cells are stem cells in adult lung. *J Clin Invest* 2013;**123**:3025−36.
9. Kapanci Y, Weibel ER, Kaplan HP, Robinson FR. Pathogenesis and reversibility of the pulmonary lesions of oxygen toxicity in monkeys. II. Ultrastructural and morphometric studies. *Lab Invest* 1969;**20**:101−18.
10. Evans MJ, Cabral LJ, Stephens RJ, Freeman G. Renewal of alveolar epithelium in the rat following exposure to $NO_2$. *Am J Pathol* 1973;**70**:175−98.
11. Hernandez-Segura A, Nehme J, Demaria M. Hallmarks of cellular senescence. *Trends Cell Biol* 2018;**28**:436−53.
12. Schafer MJ, White TA, Iijima K, Haak AJ, Ligresti G, Atkinson EJ, et al. Cellular senescence mediates fibrotic pulmonary disease. *Nat Commun* 2017;**8**:14532.
13. van Deursen JM. The role of senescent cells in ageing. *Nature* 2014;**509**:439−46.
14. Muñoz-Espín D, Serrano M. Cellular senescence: from physiology to pathology. *Nat Rev Mol Cell Biol* 2014;**15**:482−96.
15. Campisi J, d'Adda di Fagagna F. Cellular senescence: when bad things happen to good cells. *Nat Rev Mol Cell Biol* 2007;**8**:729−40.
16. Deng C, Zhang P, Harper JW, Elledge SJ, Leder P. Mice lacking p21CIP1/WAF1 undergo normal development, but are defective in G1 checkpoint control. *Cell* 1995;**82**:675−84.
17. Waldman T, Kinzler KW, Vogelstein B. P21 is necessary for the p53-mediated G1 arrest in human cancer cells. *Cancer Res* 1995;**55**:5187−90.
18. Toettcher JE, Loewer A, Ostheimer GJ, Yaffe MB, Tidor B, Lahav G. Distinct mechanisms act in concert to mediate cell cycle arrest. *Proc Natl Acad Sci U S A* 2009;**106**:785−90.
19. Jung YS, Qian Y, Chen X. Examination of the expanding pathways for the regulation of p21 expression and activity. *Cell Signal* 2010;**22**:1003−12.
20. Zon LI. Intrinsic and extrinsic control of haematopoietic stem-cell self-renewal. *Nature* 2008;**453**:306−13.
21. Milanovic M, Fan DN, Belenki D, Däbritz JH, Zhao Z, Yu Y, et al. Senescence-associated reprogramming promotes cancer stemness. *Nature* 2018;**553**:96−100.
22. Schultz MB, Sinclair DA. When stem cells grow old: phenotypes and mechanisms of stem cell aging. *Development* 2016;**143**:3−14.
23. Kuwano K, Kunitake R, Kawasaki M, Nomoto Y, Hagimoto N, Nakanishi Y, et al. P21Waf1/Cip1/Sdi1 and p53 expression in association with DNA strand breaks in idiopathic pulmonary fibrosis. *Am J Respir Crit Care Med* 1996;**154**:477−83.
24. Nagelkerke A, Span PN. Staining against phospho-H2AX ($\gamma$-H2AX) as a marker for DNA damage and genomic instability in cancer tissues and cells. *Adv Exp Med Biol* 2016;**899**:1−10.
25. Rieger ME, Zhou B, Solomon N, Sunohara M, Li C, Nguyen C, et al. P300/$\beta$-catenin interactions regulate adult progenitor cell differentiation downstream of WNT5a/protein kinase C (PKC). *J Biol Chem* 2016;**291**:6569−82.
26. Deng T, Yan G, Song X, Xie L, Zhou Y, Li J, et al. Deubiquitylation and stabilization of p21 by USP11 is critical for cell−cycle progression and DNA damage responses. *Proc Natl Acad Sci U S A* 2018;**115**:4678−83.

27. Aoshiba K, Tsuji T, Nagai A. Bleomycin induces cellular senescence in alveolar epithelial cells. *Eur Respir J* 2003;**22**:436−43.
28. Alder JK, Chen JJ, Lancaster L, Danoff S, Su SC, Cogan JD, et al. Short telomeres are a risk factor for idiopathic pulmonary fibrosis. *Proc Natl Acad Sci U S A* 2008;**105**:13051−6.
29. Naikawadi RP, Disayabutr S, Mallavia B, Donne ML, Green G, La JL, et al. Telomere dysfunction in alveolar epithelial cells causes lung remodeling and fibrosis. *JCI Insight* 2016;**1**:e86704.
30. Herbig U, Jobling WA, Chen BP, Chen DJ, Sedivy JM. Telomere shortening triggers senescence of human cells through a pathway involving ATM, p53, and p21(CIP1), but not p16(INK4a). *Mol Cell* 2004;**14**:501−13.
31. Otoupalova E, Smith S, Cheng G, Thannickal VJ. Oxidative stress in pulmonary fibrosis. *Compr Physiol* 2020;**10**:509−47.
32. Srinivas US, Tan BWQ, Vellayappan BA, Jeyasekharan AD. ROS and the DNA damage response in cancer. *Redox Biol* 2019;**25**:101084.
33. Zuo W, Zhang T, Wu DZ, Guan SP, Liew AA, Yamamoto Y, et al. $p63^{+}Krt5^{+}$ distal airway stem cells are essential for lung regeneration. *Nature* 2015;**517**:616−20.
34. Ciechanowicz A. Stem cells in lungs. *Adv Exp Med Biol* 2019;**1201**:261−74.
35. Logan CY, Nusse R. The Wnt signaling pathway in development and disease. *Annu Rev Cell Dev Biol* 2004;**20**:781−810.
36. Tian W, Li JT, Wang Z, Zhang T, Han Y, Liu YY, et al. HYD-PEP06 suppresses hepatocellular carcinoma metastasis, epithelial−mesenchymal transition and cancer stem cell-like properties by inhibiting PI3K/AKT and WNT/$\beta$-catenin signaling activation. *Acta Pharm Sin B* 2021;**11**:1592−606.
37. Rock JR, Barkauskas CE, Cronce MJ, Xue Y, Harris JR, Liang J, et al. Multiple stromal populations contribute to pulmonary fibrosis without evidence for epithelial to mesenchymal transition. *Proc Natl Acad Sci U S A* 2011;**108**:E1475−83.